Nuclear Science and Techniques **22** (2011) 282–286

Scanning transmission ion microscopy on Fudan SPM facility

LI Yongqiang[1] SATOH Takahiro[2] SHEN Hao[1,*]
ZHENG Yi[1] LI Xinyi[1] LIU Bo[1]

[1]*Institute of Modern Physics*, *Applied Ion Beam Physics Laboratory*, *Fudan University*, *Shanghai 200433*, *China*

[2]*Takasaki Advanced Radiation Research Institute*, *Japan Atomic Energy Agency*, *1233 Watanuki-machi*, *Takasaki*, *Gunma 370-1292*, *Japan*

Abstract In this paper, we report a novel measurement system based on the development of Fudan Scanning Proton Microscopy (SPM) facility. By using Si-PIN diode (Hamamatsu S1223-01) detector, scanning transmission ion microscopy (STIM) measurement system has been set up. It can provide density and structural images with high probing efficiency and non-destruction by utilizing the energy loss of high energy (MeV) and focused ions penetrating through a thin sample. STIM measurement is able to map the density distribution of organic elements which mostly compose biology materials, such information can not be detected by using conventional Be-windowed Si (Li) X-ray detector in Particle Induced X-ray Emission (PIXE) technique. The spatial resolution capability of STIM is higher than PIXE technique at same accelerator status. As a result of STIM measurement, paramecium attached on the top of Kapton tube was measured by STIM.

Key words Energy loss, STIM, PIXE, Spatial resolution, Computed tomography

1 Introduction

Numerous applications require micrometer beam spots of MeV ions. Nuclear microprobe laboratories have been making efforts to improve their spatial resolutions, which is now approaching around 100 nm[1-3] or even 10 nm[4]. For a scanning proton microcopy (SPM), studies in materials science, biological science, geological science etc can be conducted using combined ion beam analysis techniques of PIXE (particle induced X-ray emission), RBS (Rutherford backscattering spectrometry), STIM (scanning transmission ion microscopy), etc, for analysis of both minor and trace element distribution in variety of samples, organic or inorganic, homogeneous or inhomogeneous[5].

An incident ion loses its energy in a sample because of the electronic and nuclear stopping of the sample material. When MeV ions pass through a thin sample, the primary energy loss is electronic stopping, which is described by the Bethe–Bloch formula[6,7]. STIM relies on energy loss of a highly focused MeV ion beam passing through a thin sample[8]. The energy loss is converted into areal mass density, and a high quality 2D structural image of a specimen can be obtained[9].

The spatial resolution of an STIM image can achieve several micron or even less, because the transmitted ions maintain a straight path, with small scattering angles. STIM is also of high probing efficiency, low ion beam currents, non-destruction and rapid imaging[10-12].

STIM has become a versatile analytical technique for applications in materials science and life sciences[13]. Combined with computed tomography (CT), STIM allows 3D tomographic reconstruction of mass density[14,15]. STIM can be a complement to PIXE, for correcting X-ray yield in micro-PIXE analysis and accurate elemental mapping[16]. External beam STIM is used to image small living animals[17]. Ion channeling STIM is sensitive to small changes in crystal quality[18], with minimal specimen damage.

Supported by Shanghai Synchrotron Radiation Facility project

* Corresponding author. *E-mail address:* duhanwen@sinap.ac.cn

Received date: 2010-09-01

In this paper, we report our work to establish the STIM system at Fudan.

2 Experimental

The experiments were performed at the micron beam line at Fudan with a 2.0 MeV proton beam from a NEC9SDH-2 tandem accelerator. Sample holder is based on an x-y-z target manipulator (x, y: ±12.5 mm, z: 0–50 mm, step : 5 μm)[19].

A Hamamatsu Si-PIN diode S1223-01 detector, biased at 4 V, was placed behind the sample holder. The borosilicate glass window on the detector was removed to expose the active area (3.06×3.06 mm chip). The detector was connected to a charge sensitive preamplifier and a spectroscopy amplifier with the time constant of 0.5 μs. The energy resolution of the detector was 25 keV (FWHM), as measured in vacuum with 2.0 MeV proton. The details of Si-PIN diode detector is described in Ref.[20].

Figure 1 shows schematics of the STIM system. A device in Fig.2 was made to protect the detector from exposure to large beam currents. It can be moved vertically. Low beam currents (<1 f A) for STIM measurement were obtained by close collimation and object slits or lowered ion source[21].

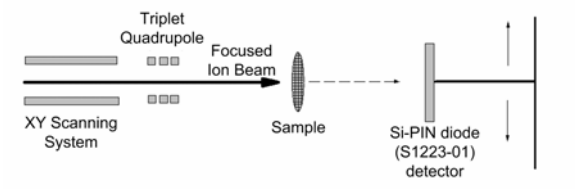

Fig.1 Layout of the STIM system with the focused ion beam. The beam scans over the sample in X and Y directions. Energy of ions passing through the sample is measured with the Si-PIN diode detector, which can be moved vertically.

Fig.2 The device that holds the detector.

A Si (Li) detector (Sirius80, Gresham Ltd.) with an energy resolution of 150 eV at 5.9 keV was positioned at 135º with respect to the beam incidence. The target-detector distance can be adjusted for various measurements.

3 Results and discussion

Figure 3a shows a PIXE spectrum collected with the Si(Li) system from a copper grid of 400 mesh with 50-μm pitches (38-μm hole and 12-μm bar). The two peaks, Cu Kα and Kβ, were used to construct the grid image (Fig.3b, 124 μm×124 μm) by correlating the peak counts with beam scan position data.

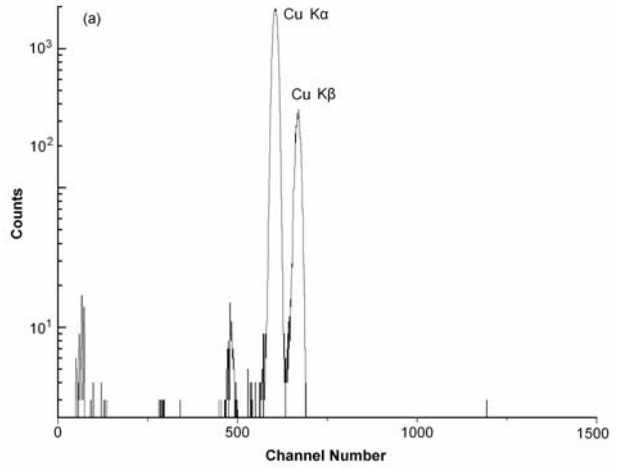

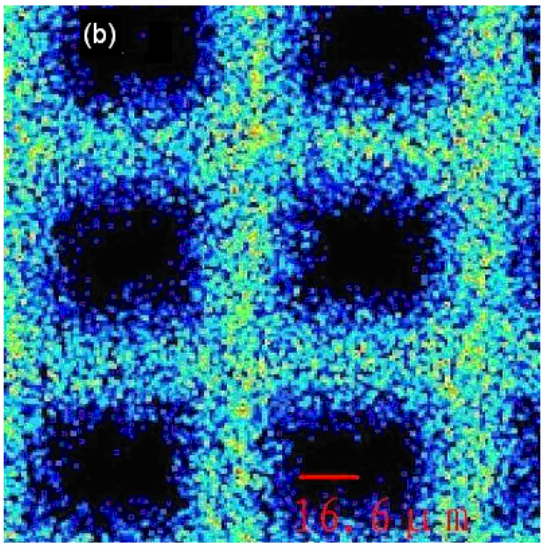

Fig.3 PIXE spectrum (a) and image (b) of a 400-mesh copper grid (124 μm×124 μm) with. 50–μm pitches (38-μm hole and 12-μm bar).

The STIM measurement with the copper grid is shown in Fig.4. Energy loss of 2 MeV protons was

obtained by the peak positions[22]. Peaks A and B were caused, respectively, by energy loss of 2 MeV protons passing certain thickness of the grid bar and the bar brim. Peak C was the incident beam energy.

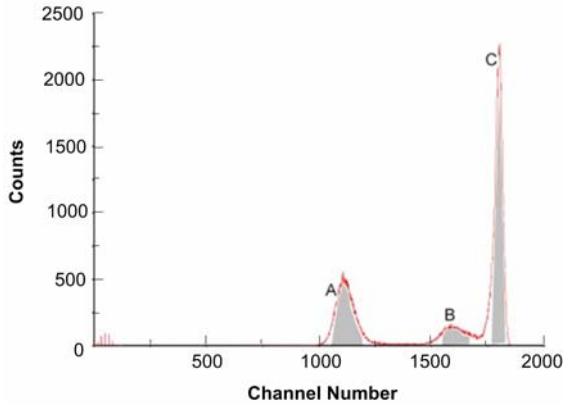

Fig.4 STIM spectra of the copper grid with 2 MeV protons. Peaks A and B were caused, respectively, by energy loss of ions passing certain thickness of the grid bar and the bar brim. Peak C was the incident beam energy (2.0 MeV).

Areal mass density (ρ_{areal}) of the grid bar is a function of the measured transmission energy.

$$\rho_{areal} = \int_0^T \rho(x)\mathrm{d}x = \int_{E_0}^{E} \left(\frac{\mathrm{d}E}{\mathrm{d}(\rho x)}\right)^{-1}\mathrm{d}E \qquad (1)$$

where T is the specimen thickness, $\rho(x)$ is its density at a depth x, dx is unit length, E_0 is the incident energy, E is energy of protons emerging from the specimen, and dE/d(ρx) is mass stopping power of the specimen. Therefore from the STIM spectrum, the thickness distribution map of copper grid could be obtained varying energy (Fig.5), where the grid bar and hole images matched together.

Widths of the peaks A, B and C are determined by energy resolution of the detection system, energy straggling, beam energy spread, etc[23-27]. Peak C, the narrowest, is determined by beam energy spread and energy resolution of the detection system. For peaks A and B energy straggling of the protons penetrating the sample makes a great contribution, in addition to the factors mentioned above.

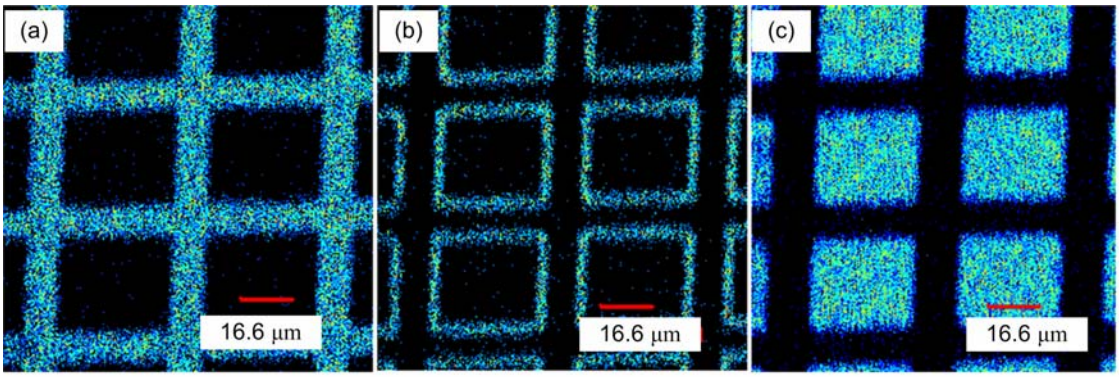

Fig.5 STIM images of the 124 μm×124 μm Cu grid, obtained by selecting the energy ranges in Fig.4 corresponding to certain thickness of the grid bar (a), brim thickness of the grid bar(b), and the grid hole (c).

Figure 6 shows the results using the beam profile monitor utility in the OM DAQ software[28]. The beam spot size could be estimated by measuring the difference between the 10% and 90% levels of counts when the beam was scanning over a grid bar. The horizontal and vertical resolutions in STIM analysis were estimated at X_2–X_1=1.9 μm and X_4–X_3=1.8 μm, respectively. In PIXE analysis, spatial resolutions in the horizontal and vertical directions were estimated at 5.1 and 4.6 μm, respectively. The slits setting needs a compromise between the beam current and beam size. Under the same accelerator status, STIM image of the Cu grid (Fig.5), which was obtained under extremely low beam current of about 0.1 fA, exhibits a higher spatial resolution than the PIXE image (Fig.4), which was collected with beam currents of about 100 pA to a few nA or larger.

Figure 7 shows a STIM spectrum of a paramecium glued with vinyl acetate on bottom of a Φ80 μm Kapton tube (the insert), consisting of carbon, hydrogen and oxygen. Peak 1 is energy of the incident protons. The lower energy part was caused by energy loss in the sample, peak passed through the tube hollow and peak passed through the tube walls. The thickness at each position could be estimated from the energy loss. Thickness variation of the sample could be derived from the spectrum. From 2-D STIM measurement results in Fig.8, the tube hollow, the tube

wall (with flaws in it), and the paramecium profile can be clearly seen.

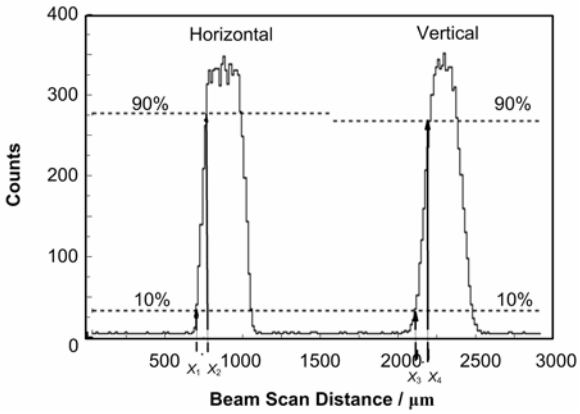

Fig.6 Beam monitor for a scanning beam over grid bars in the horizontal and vertical directions. The dashed lines denote 90% and 10% levels of counts.

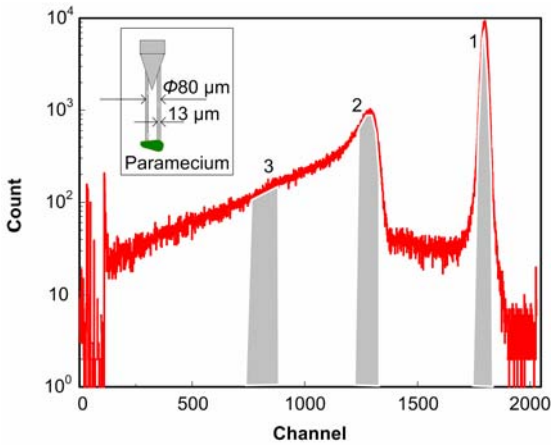

Fig.7 STIM spectra of a paramecium, glued with vinyl acetate on the top of a Kapton tube. Peak 1 was the incident energy. The lower energy parts were caused by energy losses of the protons that (1) did not pass through the sample, (2) passed through the tube hollow and (3) passed through the tube walls.

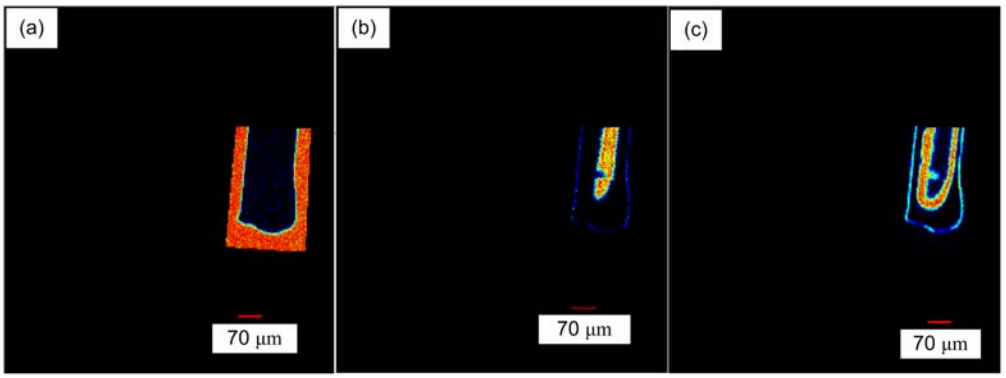

Fig.8 STIM iamges of the sample combination. (a) The tube hollow, (b) the tube wall, and profile of the paramecium (c).

4 Conclusion

The method of STIM analysis is an ideal way to image thickness distribution and structure of sample at micrometer scale using MeV protons. STIM can map organic elemental contents in sample and has a higher spatial resolution than PIXE, which measures the concentration of the inorganic major and trace elements with atomic number higher than 12 using Be-windowed Si (Li) X-ray detector. The combination of STIM and PIXE measurements at Applied Ion Beam Physics Laboratory, Fudan University, has been used simultaneously[29] to carry out a complete characteristic of major and trace element contents, and distributions. In future studies, combining the modern CT technique and other nucleus analysis technology, the 3-D analysis can be applied efficiently to the small particles without slicing the sample itself[30].

References

1 Siegele R, Kachenko A G, Ionescu M. Nucl Instrum Meth B, 2009, **267:** 2054−2059.

2 Watt F, Bettiol A A, van Kan J A. Nucl Instrum Meth B, 2009, **267:** 2113−2116.

3 Melnik K I, Magilin D V, Ponomarev A V. Nucl Instrum Meth B, 2009, **267:** 2036−2040.

4 Doyle B L, Foiles S M, Antolak A J. Nucl Instrum Meth B, 2009, **267:** 1995−1998.

5 Ren M Q. Nuclear Microscopy: Development and Applications in Atherosclerosis, Parkinson's Disease and Materials Physics. Finland: Mathematics and Natural Sciences of the University of Jyväskylä, 2007, 5−24.

6 Knoll J F. Radiation Detection and Measurement. New York (USA): Wiley press, 1989, 20−40.

7 Tang J Y, Zhang Z H. The stopping power range and channelling effect of particle passing through matter

Nuclear Energy. Beijing: Atomic energy press, 1986, 32−40.

8 Minqin R, van Kan J A, Bettiol A A. Nucl Instrum Meth B, 2007, **260:** 124−129.

9 Pontau A E, Antolak A J, Morse D H. Nucl Instrum Meth B, 1989, **40−41:** 646−650.

10 Schofield R, Lefevre H, Shaffer M. Nucl Instrum Meth B, 1989, **40–41:** 698−701.

11 Fischer B E, Mühlbauer C. Nucl Instrum Meth B, 1990, **47:** 271−282.

12 Pontau A E, Antolak A J, Morse D H. Nucl Instrum Meth B, 1991, **54:** 383−389.

13 Rothermel M, Reinert T, Andrea T. Nucl Instrum Meth B, 2010, **268:** 2001−2005.

14 Schwertner M, Sakellariou A, Reinert T. Ultramicrosopy, 2006, **106:** 574−581.

15 Wegdén M, Elfman M, Kristiansson P. Nucl Instrum Meth B, 2006, **249:** 756−759.

16 Satoh T, Oikawa M, Kamiya T. Nucl Instrum Meth B, 2009, **267:** 2125−2127.

17 Lefevre H W, Schofield R M S, Ciarlo D R. Nucl Instrum Meth B, 1991, **54:** 47−51.

18 Bench G, Saint A, Legge G J F, Cholewa M. Nucl Instrum Meth B, 1993, **77:** 175−183.

19 Zhong L, Zhuang W, Shen H. Nucl Instrum Meth B, 2007, **260:** 109−113.

20 Devès G, Matsuyama S, Barbotteau Y. Rev Sci Instrum, 2006, **77:** 056102.

21 Aguer P, Alves L C, Barberet Ph. Nucl Instrum Meth B, 2005, **231:** 292−299.

22 Ma L, Chen Q Z , Xue J M. 2008, Radiat Meas, **43:** S598−S602.

23 Szilágyi E. Nucl Instrum Meth B, 2000, **161–163:** 37−47.

24 Pászti F, Szilágyi E, Horváth Z E. Nucl Instrum Meth B, 1998, **136–138:** 533−539.

25 Amsel G, d'Artemare E, Battistig G. Nucl Instrum Meth B, 1997, **122:** 99−112.

26 Tosaki M, Ohsawa D, Isozumi Y. Nucl Instrum Meth B, 2004, **219-220:** 241−245.

27 Sigmund P. Particle penetration and radiation effects. Berlin Heidelberg (Germany): Springer press, 2005, 35−312.

28 Merchant M J, Mistry P, Browton M. Nucl Instrum Meth B, 2005, **231:** 26−31.

29 Kertész Zs, Szikszai Z, Uzonyi I. Nucl Instrum Meth B, 2005, **231:** 106−111.

30 Michelet C, Moretto Ph. Nucl Instrum Meth B, 1999, **150:** 173−178.